Computers and Electronics in Agriculture xxx (xxxx) xxxx

Contents lists available at ScienceDirect

Computers and Electronics in Agriculture

journal homepage: www.elsevier.com/locate/compag

Agricultural field shape descriptors as predictors of field efficiency for perennial grass harvesting: An empirical proof

L. Michael Griffel[a,*], Veronika Vazhnik[a,b], Damon S. Hartley[a], Jason K. Hansen[a], Mohammad Roni[a]

[a] Idaho National Laboratory, Idaho Falls, ID, USA
[b] Pennsylvania State University, State College, PA, USA

ARTICLE INFO

Keywords:
Field efficiency
Perennial grass
Bioenergy
Geographic information systems
Field boundary descriptors

ABSTRACT

Perennial grasses can serve as a material for bioenergy, biomaterials, animal feed or bedding, or other purposes. Researchers suggest that planting perennial grasses on marginal parts of agricultural fields can provide sustainability benefits; however, planting the marginal areas may result in complex shapes and changes to field areas and thus be difficult to harvest. Harvesting costs can be a limiting factor in widely adopting perennial grasses, so the more efficient the machinery operations are, the more viable perennial crops become for farmers and bioenergy stakeholders. This study explores the relationship between field shape and size and empirically derived harvesting efficiency to support assumptions relative to predicting harvesting cost, greenhouse gas (GHG) emissions, labor demands, and other factors impacting willingness to cultivate energy crops, which can be impacted by field efficiency. Switchgrass (*Panicum virgatum L.*) mowing data were used in the study. The regression analysis showed that the natural log transformation of the perimeter-to-area (P/A) ratio was the most accurate predictor for field efficiency (FE) (R^2 = 71%) among shape descriptors as it takes both field size and shape into account. Optimizing field designs that combine annual crops and perennial grasses for lower P/A ratios will decrease operation costs and, thus, improve the rate of practice adoption of perennial grasses in agriculture.

1. Introduction

Perennial grasses, like switchgrass (*Panicum virgatum L.*), are an alternative to current crop rotation that can supply feedstock to the emerging bioeconomy. Grasses can produce biomass for bioenergy conversion (McLaughlin and Kszos, 2005), biomaterials like bio-based polymers and composites (Bilal et al., 2017; Isikgor and Becer, 2015), and many other uses. The 2016 Billion-Ton Report (Langholtz et al., 2016) demonstrated that switchgrass and other grasses could be established across the U.S., including in states where annual crops dominate agriculture, and would create both a supply and new markets for biomass resources.

Beyond possible market and economic benefits, changing from annual crops to perennial grasses reduces farm nutrient and sediment runoff, especially on marginal land (Brandes et al., 2018; Cibin et al., 2016). Compared to annual cropping systems, perennial grasses increase bird species richness and density (Robertson et al., 2011) and increase the diversity of plant and animal species, pollinators, and methanotrophs (Schulte et al., 2017; Werling et al., 2014). Overall, perennial systems require fewer nutrient and chemical inputs than annual systems, making the environmental footprint of perennial grasses lower than those of annual crops (Parrish and Fike, 2005).

Apart from local benefits to water and soil quality, perennial cropping systems can help reduce carbon emissions, which could have a global impact. Switchgrass cropping systems sequester higher levels of soil organic carbon (SOC) in both shallow (i.e., 0–30 cm) and deeper (> 30 cm) soils compared to nearby croplands used to produce annual crops (Liebig et al., 2005). An assessment of potential use of marginal lands for perennial grasses in ten Midwestern U.S. states showed that such systems not only mitigate GHG emissions at a rate comparable to traditional agricultural crops, but also have the potential to produce approximately 63 GJ of energy in ethanol per hectare annually (Gelfand et al., 2013). Because of this potential, perennial grasses create a carbon-negative energy system.

To ensure that food security and current agricultural supply chains are not affected, researchers suggest substituting annual crops for perennial grasses only on marginal parts of the fields, leaving the annual crop rotation on the non-marginal subfields. For this analysis, subfields

* Corresponding author.
E-mail address: mike.griffel@inl.gov (L.M. Griffel).

https://doi.org/10.1016/j.compag.2019.105088
Received 29 May 2019; Received in revised form 7 October 2019; Accepted 2 November 2019

are smaller parts of the field exhibiting different soil characteristics, topography, and other attributes influencing crop yields. Marginality is usually defined as chronically low annual crop yield and no return on investment. Low-yielding land often has high erosion and runoff potential, and perennial grasses can help protect the soil from eroding while producing enough biomass for alternative energy production (Bonner et al., 2016; Nair et al., 2018). The resulting field that combines annual and perennial grasses is an example of integrated landscape management (ILM). ILM integrates functions that different crops and practices carry; for example, an ILM design might combine food and bioenergy crops because the different end products (Ha and Wu, 2015; Ssegane and Negri, 2016) or plants provide multiple ecosystem services that are sought after by different stakeholders connected to the landscape (Estrada-Carmona et al., 2014; Sayer et al., 2013). Usually, ILM designs call for different types of crops or practices in different subfields.

However, the viability of integrating annual and perennial farming systems within single agricultural fields partially depends on the efficiency of crop planting and harvesting. Marginal subfields can be irregular in shape and area and difficult to access given they are typically defined by soil and topography features. That means that machinery operations on some parts of the field could be infeasible. Efficient field designs are the key to balancing costs and ecosystem services in perennial systems.

Like forage crops, tall perennial grasses require seeding, crop inputs (e.g., fertilizer), mowing, conditioning, raking, and baling operations (Sokhansanj et al., 2009). Each agricultural operation can have inefficiencies connected to its respective machine. Mowing is the operation that most closely follows the shape of the field, which is why it is the focus of this study. Switchgrass can be mowed using hay equipment like disc-type mowers or swinging flail blade mowers (Douglas et al., 2009), which is studied in this paper.

Efficiency can be expressed in a variety of ways, for example, machinery fuel efficiency, amount of spatial overlap, ratio between speed of harvest and yield, and many others. Effectiveness—the percent of the area covered by the machinery without gaps or overlaps—can be one of the measures to compare performance, but it requires very precise spatial data, which are seldom available from operators. Time-based efficiency measures can be more practical in the field because they require less equipment calibration. These are the focus of this analysis. Time-based FE affects feedstock-logistics cost. A lower FE implies more time in breaks and suggests low average field speed of harvesting equipment. The low field speed of harvesting equipment increases harvesting time, which ultimately contributes to higher harvesting cost due to increased labor time, fuel consumption, and, potentially, additional equipment and maintenance costs.

This study uses a time-dependent FE measure, as standardized by the ASAE EP496.3 (American Society of Agricultural and Biological Engineers, 2015). Field efficiency is defined as the ratio between the real and the theoretical productivity of a machine. In the case of harvesting equipment, efficiency is often expressed as the ratio between productive time and the total time in the field. For this study, FE is calculated using Eq. (1):

$$FE = \frac{T_{work}}{T_{work} + T_{breaks}} \quad (1)$$

where T_{work} (time for delay-free work) is the time to complete the operation with no delays or disengagement, and T_{breaks} (time disengaged during breaks) is the time spent when the equipment is disengaged due to turning or navigating around obstacles and traveling in the headland space. T_{breaks} is likely impacted by field area and geometry, which affect the time spent turning while disengaged, the number of turns required during the operation at headlands or for navigating around obstructions, and the distance traveled in the headland space.

Accurate FE measurements are critical to improved understanding of agricultural field operations and logistics impacts on overall economics, environmental, and labor costs. Such impacts are relevant to both bioenergy stakeholders and agricultural producers. Analysis of spatiotemporal field operations data from 52 agricultural fields with varying area and shape complexity showed the percentage of double-planted areas ranged from 0.1% to 15.5%, and potential economic losses ranging from $4–26/ha could be mitigated with advanced control systems (Velandia et al., 2013). FE helps to quantify the variation of harvest and collection costs from one field to another, involving multiple pieces of harvesting equipment, such as mowers, rakes, and field-conditioning equipment (Roni et al., 2018). FE is also a critical metric to assess subfield design within an integrated landscape management practice. Finally, FE is essential to accurately predict GHG emissions during harvesting from different fields (Cai et al., 2018).

Previous analysis indicates that the shape and size of the field/subfield and the presence of in-field obstructions can serve as indicators of machinery-movement effectiveness (spatial overlap) and efficiency (time spent in headland turns and around in-field obstructions). A study of the statistical relationship of multiple field-boundary shape descriptors and agricultural sprayer coverage data showed the field P/A ratio had the strongest relationship with sprayer overlap error (% of field area overlapped). Regression analysis shows surface area descriptors and combined shape and size indices are useful to guide land parcel consolidation decisions and to optimize machinery movement patterns (Gonzalez et al., 2004; Luck et al., 2011). Researchers proposed a planning method based on the traveling salesman problem (TSP) to develop area equipment coverage plans to optimize FE for fields that had irregular boundaries and in-field obstructions (Zhou et al., 2014).

Additional studies have used simulation to model the relationship between FE and field geometry where empirical equipment data are not publicly available and must be obtained via agricultural industry contacts or other sources. For example, Oksanen examined approximately 65,000 field parcels to evaluate varying shape indices relative to field classification. The author then linked the indices to modeled FE calculated based on the time spent in headland turns, which he simulated (Oksanen, 2013). Wold et al. developed a MATLAB program to simulate grain harvest and residue collection operations to evaluate grain collection and field operations efficiency (Wold et al., 2011). Researchers compared simulation results to real-world harvester data and found estimates of harvest capacity differed by only 6.5%. By using current empirical data to study how field geometry affects the FE of harvesting, this study aims to build upon the current body of knowledge and support feedstock logistics assumptions for biomass harvest operations. This work contributes to the literature in that it incorporates high spatiotemporal resolution data (1-second intervals) derived from real-world switchgrass cutting operations and demonstrates a strong statistical relationship to simple field area and boundary descriptors. The statistical relationships outlined in this paper will provide a path forward for other researchers to estimate switchgrass cutting operational efficiencies using simple field boundary descriptors that can be generated using publicly available data when empirical data are not available, thereby strengthening downstream analysis.

The goal of this analysis is to evaluate the relationship between field geometry and harvest FE. This analysis differentiates from many previous studies in that it is not intended to optimize field coverage pathways. Instead, the aim is to quantify FE of current field operations. This research focuses on switchgrass mowing in fields of varying sizes and shapes. To reach this goal, researchers quantify FE from available empirical data from the equipment field coverage data utilizing regression analysis to find whether field boundary shape and area descriptors can explain field efficiency variation between fields. These findings introduce a simplified approach to predict FE using shape indices to support agricultural integrated landscape designs without having empirical data on switchgrass cutting coverage.

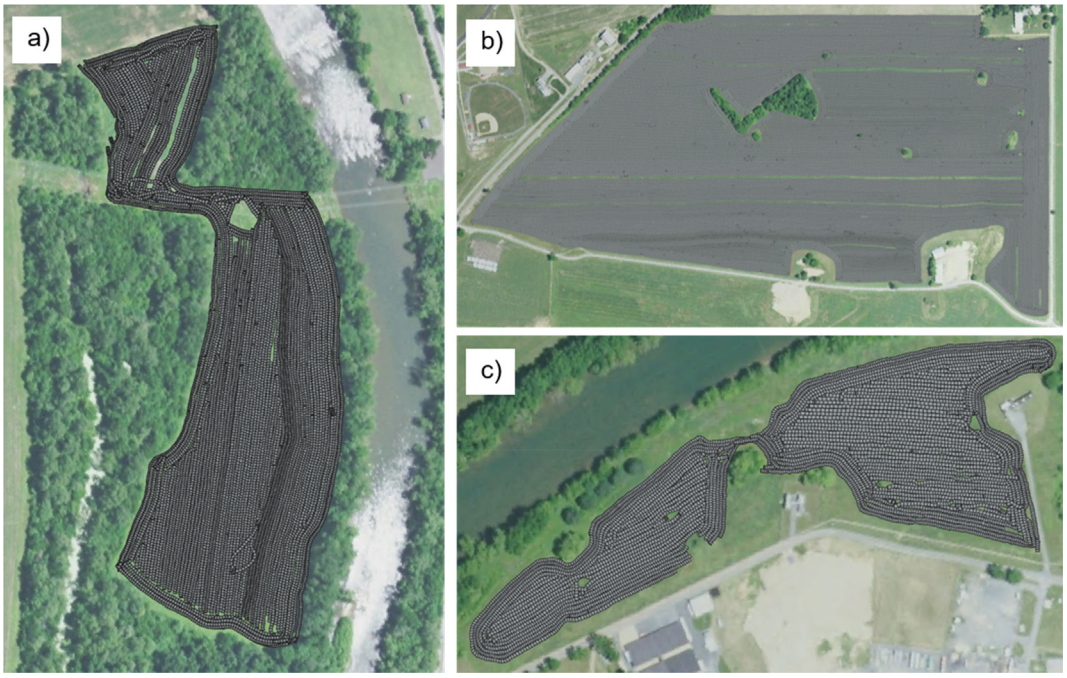

Fig. 1. Three fields with switchgrass mowing coverage data collected with GPS-equipped computer controllers. The individual polygons represent areas covered by the equipment in one-second intervals. The background imagery is derived from the National Agriculture Imagery Program (NAIP) data, collected at a 1-meter spatial resolution during the 2016 crop production year.

2. Materials and methods

2.1. Field data collection

Geo-referenced data of switchgrass mowing coverage were collected using agricultural equipment at the end of the 2017 growing season in the eastern United States by FDC Enterprises Inc. (New Albany, Ohio). The data spanned 70 fields, totaling 441.7 ha. The equipment consisted of tractors equipped with mowers either 3 or 3.35 m in width and Raven Envisio Pro controllers (Raven Applied Technology, Sioux Falls, South Dakota) data acquisition systems (DAS). These controllers are used within the agricultural industry to log equipment movement patterns and control site-specific crop input rates during variable rate applications. These data were exported as polygon shapefiles in the World Geodetic System (WGS 84, EPSG:4326) coordinate system. Each polygon represents the coverage area associated with each recorded instance spanning one second. Fig. 1 shows a map of three fields with overlaying switchgrass cutting coverage data. The following time-series animations (Fig. 1_a.gif, Fig. 1_b.gif, & Fig. 1_c.gif) show the actual machine movement for the switchgrass harvesting operations displayed in Fig. 1.

The DASs were equipped with Global Navigation Satellite System (GNSS) receivers that return equipment's longitude, latitude, and elevation positions. The data in GNSS receivers are corrected via the Wide Area Augmentation System (WAAS) to generate accuracies of approximately ± 3 m about 95% of the time (United States Department of Transporation, 2008). The DASs were set up to log machinery position at one-second intervals, which is hereafter referred to as time-series data. For the complete list of attributes, see Table 1. The system only recorded spatial information while the mowing equipment was engaged and did not log these features while the equipment was disengaged—i.e., when turning in headlands, navigating obstructions, or shut down for maintenance or other breaks.

For this analysis, the timestamp feature, shown in Table 1, was used to quantify FE, as described by Eq. (1). The timestamp feature records the current date and time in seconds as an integer value. Given that FE in this analysis only accounts for temporal disparities related to field navigation, no other feature records were utilized in this analysis.

Table 1
Data collected with Raven Envision Pro controllers during switchgrass harvesting operations.

Feature	Description
timestamp	The number of seconds having occurred since January 1, 2006.
areaSqM	The area of the polygon in square meters corresponding to the data instance.
cog	The current compass heading in degrees.
sogMperSec	The current machine speed in meters per second.
elevM	The elevation in meters at the time of recording.
antennaLat	The latitude of the receiver antenna in degrees.
antennaLon	The longitude of the receiver antenna in degrees.
rate	The current product application rate in gallons per acre.
targetrate	The target product application rate in gallons per acre.

All field boundaries were digitized by hand using QGIS geographic information system (GIS) software (QGIS Development Team, 2018) based on the switchgrass harvest coverage data and United States Department of Agriculture (USDA) National Agricultural Imagery Program (NAIP) data, collected at a 1-meter spatial resolution during the 2016 growing season. Field boundary digitization closely approximated the switchgrass cutting coverage data, including in-field obstructions prohibiting operation (Fig. 2). This process generated 70 field boundaries that were saved as polygon shapefiles using the NAD83 (2011)/Conus Albers (EPSG:6350) coordinate system to support meter-based length and area calculations when deriving boundary shape descriptors. The area of the digitized fields ranged from 0.4 to 65.5 ha with a mean area of 6.3 ha.

2.2. Empirical field efficiency

To quantify empirical FE based on Eq. (1), we first identified polygons near turns that were later used to calculate T_{breaks}. Visual examination of the cutting data showed operators made several headland passes around the contours of a field (typically six passes) and then transitioned to parallel back-and-forth passes to cover the interior

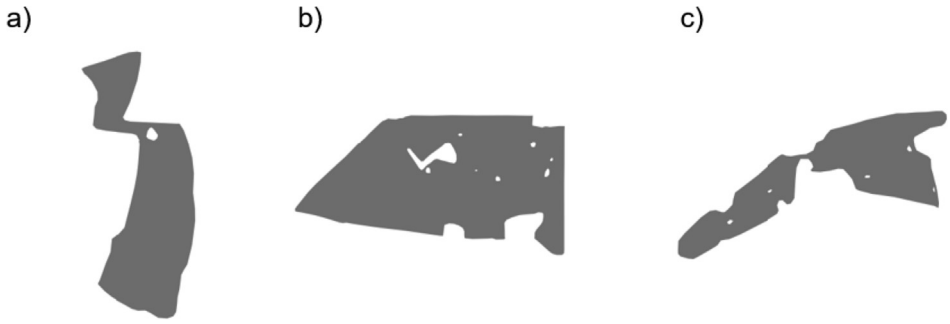

Fig. 2. Three of the 70 manually digitized field boundaries showing varying complexity relative to shape and size where the area of each spans (a) 8.2 ha, (b) 51.2 ha, and (c) 4.2 ha.

section (Fig. 1). The turns needed to maintain such patterns required that equipment be disengaged with acute to straight turning angles. Additionally, field obstructions of varying sizes, like patches of trees or rocky outcroppings, meant the equipment was disengaged to navigate around those obstructions and then resumed the original equipment heading.

Because equipment disengagement and navigation can occur with no change in equipment heading, researchers chose to quantify FE based on the timing of the breaks, rather than the angle of turns. T_{work} was calculated by summing the total number polygons in each field, that sum equaled the total number of seconds to mow switchgrass in the field. Because the switchgrass coverage data consisted of 766,985 polygons (70 fields), this processing was automated using Python 3.6 and the GeoPandas 0.3.0 library. FE was calculated per Eq. (1), using the time machines spent working and the break times.

To calculate the time for breaks, we calculated differences between timestamps of temporally adjacent polygons. Those with differences greater than or equal to 10 s and less than or equal to 90 s were included in the T_{breaks} summation. (Fig. 3a). A 10-second gap was used as the minimum time needed for a break because equipment turns in less than 10 s are unlikely. A maximum gap for a break was set to 90 s as disengagement periods longer than 90 s likely were breaks unrelated to field geometry; rather, they were due to maintenance or operator breaks. All turn-related break times were summed for each field and were equal to the total time in seconds that the equipment spent in a disengaged state navigating turns and in-field obstructions (T_{breaks}). All polygons that satisfied the break criteria of 10 s ≤ Time Gap ≤ 90 s were labeled in QGIS to visually verify this method for computing time breaks (Fig. 3b).

2.3. Field boundary shape and area descriptors

We used eight spatial descriptors to characterize the seventy fields for regression analysis. The spatial descriptors included area, perimeter, P/A ratio, convexity, compactness, rectangularity, square-perimeter index, and curb index. These measures are described in the following section. Calculation of the field descriptors was automated using Python 3.6 and the GeoPandas 0.3.0 software library.

Field boundary area and perimeter values were calculated as meters-squared (m^2) and meters (m), respectively, using native GeoPandas area and perimeter functions. In-field obstructions were excluded from the total area calculation; perimeter length was added as interior field boundaries. The remaining independent variables were derived based on Eqs. (2)–(7), utilizing area and perimeter features.

The ratio of the P/A (m^{-1}) was calculated per Eq. (2) (Luck et al., 2011).

$$\frac{P}{A} = \frac{Perimeter}{Area} \tag{2}$$

Convexity is a unitless metric that defines how closely a polygon matches a convex architecture and was calculated as a ratio between total area and convex hull area, shown as Eq. (3) (Oksanen, 2013). The convex hull area is the area of the smallest convex polygon encompassing the original polygon.

$$Convexity = \frac{Area}{Convex\ \ Hull\ \ Area} \tag{3}$$

Compactness is a unitless measure of how circular a polygon shape is. It is calculated as in Eq. (4) (Oksanen, 2013).

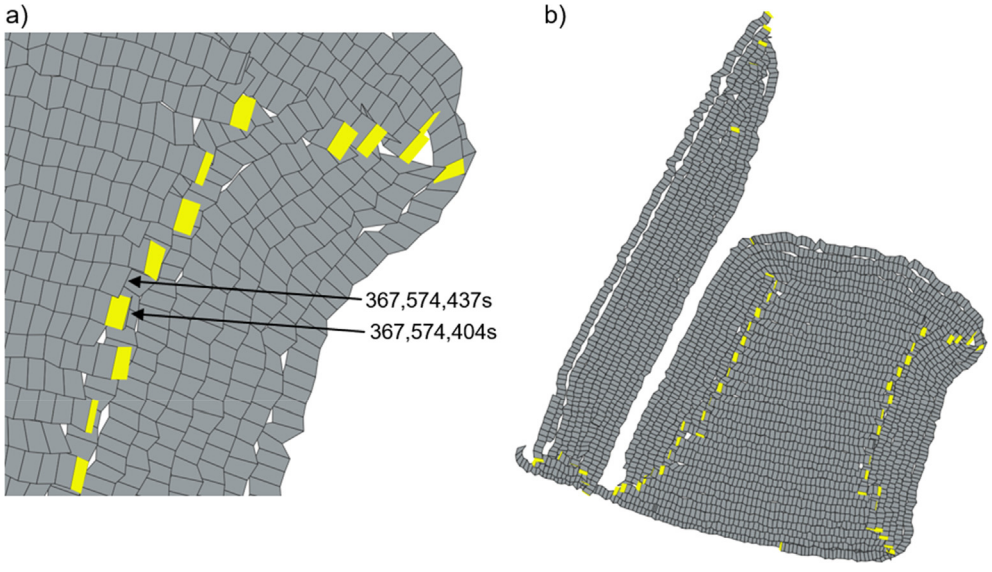

Fig. 3. (a) Switchgrass mowing coverage (gray) with yellow polygons illustrating the last polygon at the end of a pass. The integer values represent the timestamp value associated with individual polygons at the end of one pass and the beginning of the next pass. (b) The turning polygons (yellow) of one field; as expected, the turns are in headland areas. (For interpretation of the references to colour in this figure legend, the reader is referred to the web version of this article.)

$$Compactness = 4\pi \frac{Area}{Perimeter^2} \quad (4)$$

Rectangularity (unitless) indicates the rectilinearity of a polygon based on its relationship to the polygon's minimum bounding rectangle area. It is calculated based on Eq. (5) (Oksanen, 2013; Toussaint, 1983). The minimum bounding rectangle area is derived from the area of the smallest rectangular polygon that can encompass the original polygon.

$$Rectangularity = \frac{Area}{Minimum\ \ Bounding\ \ Rectangle\ \ Area} \quad (5)$$

The unitless square-perimeter index (SPI) quantifies the relationship of a boundary perimeter to the perimeter of a square with the same area as shown by Eq. (6) (Luck et al., 2011).

$$SPI = \frac{4 \times \sqrt{Area}}{Perimeter} \quad (6)$$

The unitless curb index (CI) defines the ratio of the headland area to the total area of the field, as in Eq. (7). The index was developed to represent equipment coverage strategies for which operators utilize multiple headland passes before transitioning to a parallel back-and-forth pattern, such as those seen in the switchgrass cutting data used in this analysis (Oksanen, 2013).

$$CI = \frac{Area - Offset\ \ area}{Area} \quad (7)$$

The offset area is calculated from the number of passes in headland areas and the width of the equipment. The headland area is the product of equipment width and the number of passes. That area was drawn as a buffer around field boundaries in the QGIS software. For this analysis, the number of passes for each field was specified by counting the passes along with specific equipment widths (3 or 3.35 m) to calculate the CI for each field.

As illustrated in Fig. 2, some fields also included areas within boundaries obstructing machinery operations and are represented as holes within the polygon geometry. Those obstructions (like trees) were considered in field boundary descriptor calculations. For example, the perimeter of the in-field obstructions was included in the total perimeter of the field, but the area of those obstacles was subtracted from the total area.

2.4. Statistical analysis

After compiling FE values by field using the switchgrass cutting data and field boundary descriptors based on the manually digitized field polygons, the data were compiled for ordinary least squares (OLS) linear regression analysis using Python 3.6, and the software libraries named scikit-learn 0.20.2 and statsmodels 0.9.0 (Pedregosa et al., 2011; Seabold and Perktold, 2010). Because the goal of the study was to find a simple predictor of FE that can be used by managers, indices were considered separately in single variable regression. Such an approach helped avoid collinearity between predictors because many of the field descriptors were derived from area and perimeter. Also, previous research has shown multi-variable regression analysis using varying shape descriptor indices derived from field boundary perimeter and area metrics did not lead to significant model improvement (Luck et al., 2011).

Ordinary least square regression analysis was carried out, formulating the results with the generalized form of the single-variable regression equation as in Eq. (8).

$$Y = \beta_0 + \beta_1 X_1 \quad (8)$$

In this case, Y represents FE, X_1 represents a field descriptor as an independent variable, β_1 represents the coefficient describing the size of the effect of the independent variable, and β_0 represents the y-axis intercept.

Regression residuals were examined to satisfy the assumptions of linear regression. If heteroscedasticity of residuals was observed, researchers applied a logarithmic transformation to check whether the model still violated the assumptions. To maintain the no-multicollinearity assumption, the regression was carried out on each explanatory variable separately.

The Durbin-Watson test was used to evaluate autocorrelation among residuals and to test the independent observation assumption of linear regression. In our case, since n = 70 and k = 2, the lower bound and upper bounds for the test are 1.400 and 1.514 (1% significance points). Thus, if the test value is higher than the upper bound, then fail to reject the no autocorrelation hypothesis, i.e., assume that no autocorrelation is confirmed.

Given that the empirical data contained equipment either 3 or 3.5 m in width, we included this feature as one of the predictors in a multivariate regression with the field boundary descriptor that performed best in the univariate analysis. This was done to test the statistical significance of the equipment width for this specific method to model FE.

3. Results

Harvesting FE for the 70 fields of switchgrass cutting operations ranges from 0.46 to 0.92 (mean = 0.69 ± 0.09). Based on the manually digitized field boundaries, eight initial independent variables were generated for each of the 70 fields. Table 2 lists the descriptive statistics for each field descriptor.

To understand how the field geometry descriptors relate to each other, as well as to FE, researchers produced a matrix of correlation plots which is presented in Fig. 4. The plot also includes bar histograms of each feature to illustrate data distribution patterns. The matrix plots illustrate that several field descriptors are strongly correlated to each other—for example, compactness and the SPI, or P/A ratio and CI. This suggests that single-predictor regression is appropriate for this study because it helps avoid collinearity between predictors.

Review of the correlation plots in Fig. 4 indicates that CI and P/A ratio are potentially related to FE with near-normal distributions. The correlation plots also indicate area and perimeter have potentially strong logarithmic relationships with FE. Natural logarithm transformations of field area (ln area) and perimeter (ln perimeter) were performed to generate new independent variables for the regression analysis. Additional natural logarithm transformations were applied to CI (ln CI), P/A (ln P/A), and FE (ln FE) given the potential for occurrence of heteroscedasticity apparent in the correlation plots. For the descriptive statistics of the transformed variables, see Table 3. Other field descriptors, like convexity, compactness, rectangularity, and SPI, showed much weaker correlations to FE and were not included in the regression analysis.

For this analysis, eight ordinary least squares regression models were developed to quantify potential FE predictive capabilities using the independent variables identified in the previous section including CI, ln area, ln perimeter, and P/A ratio. Given the potential heteroscedasticity of CI and P/A, additional models were developed to predict

Table 2
Descriptive statistics for field boundary descriptors.

Field Boundary Descriptor	Mean	Standard Deviation	Minimum Value	Maximum Value
Area (m^2)	63103.05	108392.09	3897.92	655468.45
Perimeter (m)	1169.80	892.69	340.26	4703.83
Convexity	0.83	0.12	0.46	0.99
Compactness	0.49	0.19	0.18	0.86
Rectangularity	0.63	0.12	0.30	0.88
P/A (m^{-1})	0.03	0.02	0.01	0.09
SPI	0.78	0.16	0.47	1.05
CI	0.55	0.19	0.10	0.97

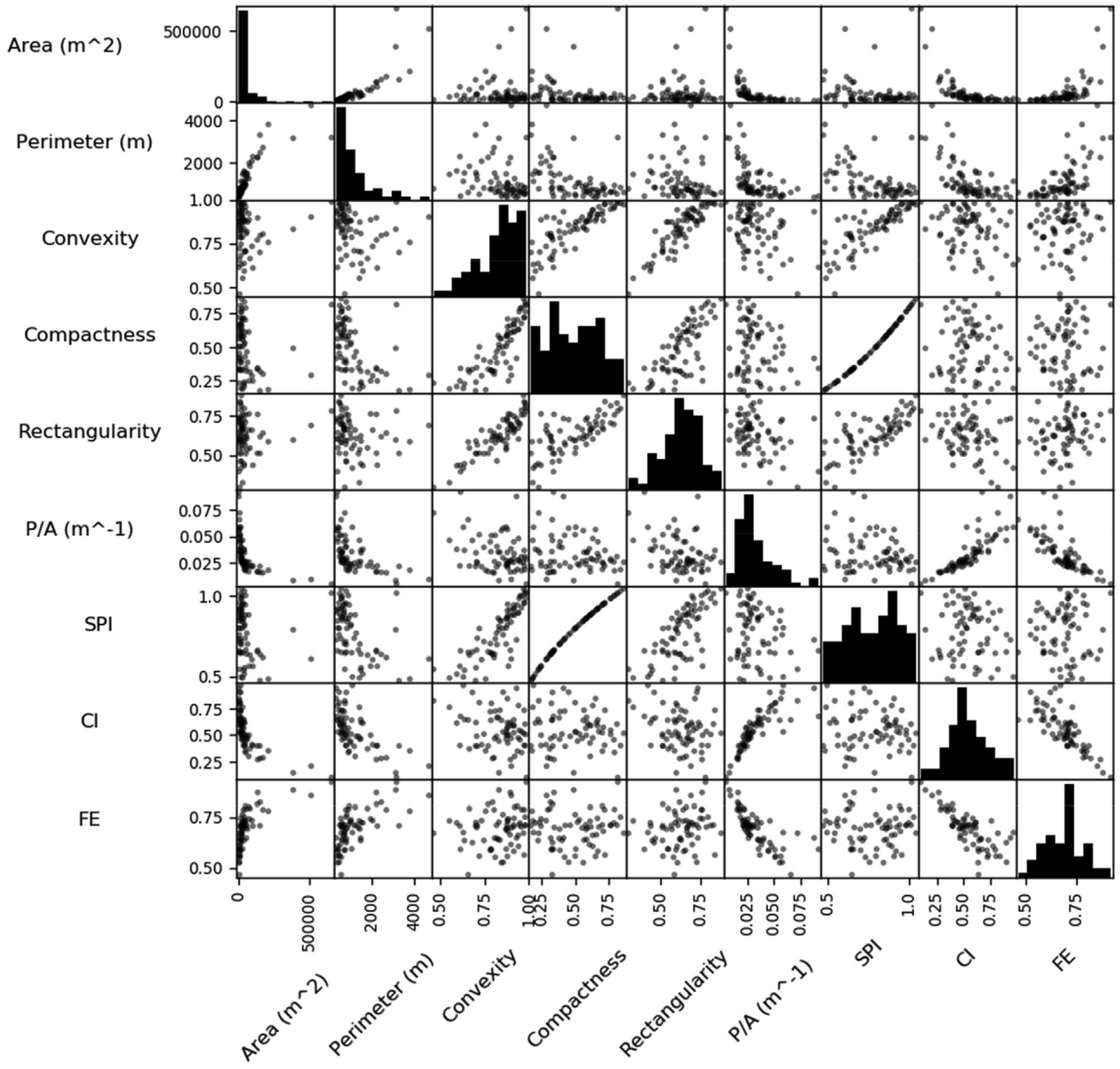

Fig. 4. Matrix of correlation plots of field boundary shape descriptors and FE.

Table 3
Descriptive statistics for the transformed explanatory variables based on the original field boundary descriptors.

Field Boundary Descriptor	Mean	Standard Deviation	Minimum Value	Maximum Value
ln Area	10.37	1.07	8.27	13.39
ln Perimeter	6.85	0.63	5.83	8.46
ln CI	−0.67	0.41	−2.31	−0.03
ln P/A	−3.52	0.52	−5.33	−2.38
ln FE	−0.38	0.13	−0.77	−0.08

Table 4
Linear (OLS) regression results.

OLS Model	β_0 *(std. error)*	β_1 *(std. error)*	R^2	Durbin-Watson
$FE = \beta_0 + \beta_1 CI$	0.898*** *(0.021)*	−0.378*** *(0.037)*	0.609	1.374
$FE = \beta_0 + \beta_1 lnArea$	−0.030 *(0.059)*	0.070*** *(0.006)*	0.689	1.242
$FE = \beta_0 + \beta_1 lnPerimeter$	−0.005 *(0.083)*	0.102*** *(0.012)*	0.508	1.189
$FE = \beta_0 + \beta_1 (P/A)$	0.821*** *(0.016)*	−3.904*** *(0.418)*	0.562	1.587
$FE = \beta_0 + \beta_1 lnCI$	0.572*** *(0.012)*	−0.177*** *(0.016)*	0.650	1.481
FE* = β_0 + β_1*lnP/A	**0.179*** *(0.040)***	**−0.145*** *(0.011)***	**0.714**	**1.548**
$lnFE = \beta_0 + \beta_1 lnCI$	−0.546*** *(0.020)*	−0.249*** *(0.025)*	0.591	1.510
$lnFE = \beta_0 + \beta_1 lnP/A$	−1.117*** *(0.062)*	−0.209*** *(0.017)*	0.681	1.561

*0.1, **0.05, ***0.01 (the probability that a Type I error has occurred).

FE and ln FE, based on ln CI and ln P/A ratio to evaluate if semi-log or log-log linear regression models demonstrated an improved fit for the data. Table 4 shows the models and OLS regression results.

The results in Table 4 illustrate that the linear model with logarithmically transformed P/A ratio has the best fit compared to other predictors (bold font). The R^2 for that model is 71%, which is a good fit for the data given the possible data-collection errors and unforeseen influences of human operators. Such errors could be related to the timing of when the operator engages and disengages the equipment, or to equipment logging inaccuracies. The multivariate regression analysis incorporating ln P/A and equipment width as independent variables showed equipment width was not statistically significant. To see the scatter plot of the ln P/A data, see Fig. 5a.

Perimeter to area ratio, both logarithmically transformed and not, is the only factor that passed Durbin-Watson autocorrelation test (for the

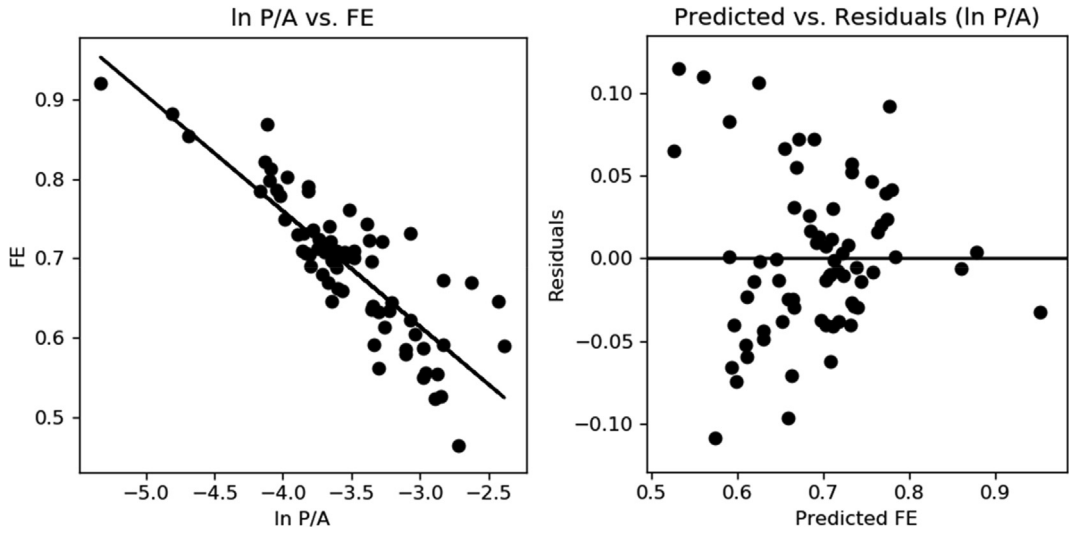

Fig. 5. (a) Logarithmic transformation of the P/A ratio regression plot to FE; (b) Plot of the residuals for ln P/A regression model.

plot of residuals, see Fig. 5b). The results for ln CI are inconclusive, and the test suggests autocorrelation is present for all other predictors; thus, they do not fulfill the independent observation assumption. Model fit and the autocorrelation tests suggest that ln P/A is a useful predictor for field efficiency in harvesting switchgrass. Fig. 5a and the regression model from Table 4 indicate that a lower P/A ratio should be targeted to achieve the highest FE.

4. Discussion

The regression analysis suggests that spatial field descriptors are useful predictors of FE. Nevertheless, not all predictors are as fitting as others. Even though most of the eight indicators are based on area or perimeter, the P/A ratio has the best fit, possibly because it represents both the size and shape of the field. It is understandable that both factors are needed to characterize a field geometry: the larger the area, the more time is spent in parallel passes compared to turns or headland passes, making the operation more efficient; similarly, the simpler the shape of the field, the fewer turns the machinery must make to cover the entire area. Given that the equipment width directly influences the number of passes and turns required to cover a field, it is likely this relationship would remain consistent over changing equipment widths. This could explain why the multivariate regression analysis showed equipment width is not statistically significant for this method of calculating FE.

Empirical data presented in the results highlight the importance of calculating field-specific machinery FE. The range in FE, from 0.46 to 0.92, illustrates that assuming the same efficiency in all fields (e.g., 0.8 is a value commonly used as the default) would lead to inaccurate calculations of machinery-related costs and emissions. Furthermore, the understanding of how field shapes affect harvesting time in each field can help optimize the field design for higher efficiency.

The approach of using timestamps to calculate field efficiency has several advantages over the space-dependent calculations that are used in the literature. Because time-steps are the metric used for efficiency calculation versus spatial overlap or gaps, the spatial error of the GPS receiver does not affect the efficiency calculation. Most of the agricultural machinery does not have very high-precision equipment, so this study's approach will be more widely applicable in operations. Similarly, even though equipment width varies between the fields in the study, that does not affect the efficiency calculation using time stamps, making the approach applicable to other agricultural operations or pieces of machinery.

Where many previous studies have not incorporated empirical data, these results will be useful for landscape planning and decision-making in integrated landscape management designs. Those designs would have to balance the shape and size of the subfields that are assigned to perennial grasses to avoid unproductive turning time. It is important to note that managers and planners will have to consider equipment width to set the minimum size of the perennial grass plots and not just count on the ratio between perimeter and the area, since the machinery should be able to make a pass or a turn in the given plot. It is important to note that accessing additional empirical spatiotemporal data related to switchgrass cutting operations would strengthen the analysis and potentially support more sophisticated approaches incorporating machine learning and computer vision techniques.

Agricultural land management often requires multiple field operations within a given year. Switchgrass cultivation for bioenergy production would require at least one seeding operation to establish the crop and likely require fertilizer and herbicide applications to maximize biomass productivity on an annual basis. In addition to annual cutting operations, harvest and collection would also likely require conditioning, raking, and baling operations. Empirical datasets derived from these field operations, could support the development of additional modelling capabilities to quantify the aggregate impacts of field shape and size on FE and resultant management costs.

Further research is needed to evaluate the FE and field geometry relationship in annual crops like maize and soybeans. The dependency between FE and harvesting operations in annual crops can be different from perennial systems because of the alternative machinery used to harvest annual grains. Understanding the FE patterns of annual crops will help design integrated landscape designs that optimize for the highest efficiency of operation with both grasses and annual crops, decreasing the possible logistics costs and encouraging the adoption of the integrated landscape design approach.

Perennial grass crop management could also require specialized field equipment that may not be part of a farmer's existing portfolio. This could influence whether a farmer chooses to integrate grass crops in lieu of current annual crops both on marginal subfield areas and on entire fields. A farmer could choose to purchase the necessary equipment or utilize third-party operators with their own equipment suited for perennial grass crop management. It is also possible that farmers currently producing perennial forage crops such as alfalfa would already have much of the equipment necessary for perennial grass crop management. Comparison between the efficiencies of managing perennial grass crops by specialized third-party operators, farmers using existing equipment, and those adding equipment to existing fleets could further enhance perennial bioenergy crop harvest and logistics

modelling.

5. Conclusion

This study used empirical data to evaluate the relationship between harvesting field efficiency in switchgrass fields and the geometry characteristics of those fields. This study showed that perimeter-to-area ratio is a useful predictor of FE because it accounts both for the size and the shape of the field. Furthermore, authors use empirical data to illustrate that setting FE to a default value for all fields is inaccurate because of the broad range of the FEs, depending on the field characteristics. The results of this study will provide more accurate FE assumptions to support feedstock logistics modelling of switchgrass from fields that have varying shape and size. In the absence of detailed empirical harvesting data, the relationships observed in this study can be used to support modelling of harvesting costs, fuel use, labor demands, and GHG emissions using simple GIS techniques.

Declaration of Competing Interest

The authors declare that they have no known competing financial interests or personal relationships that could have appeared to influence the work reported in this paper.

Acknowledgements

This work was supported by the US Department of Energy's Office of Energy Efficiency and Renewable Energy, Bioenergy Technologies Office, under DOE Idaho Operations Office Contract DE-AC07-05ID14517. Accordingly, the US Government retains a nonexclusive, royalty-free license to publish or reproduce the published form of this contribution, or allow others to do so, for US Government purposes.

The authors thank the Antares Group and FDC Enterprises for their generous sponsoring support through a cooperative agreement with the U.S. Department of Energy titled: "Enabling Sustainable Landscape Design for Continual Improvement of Operating Bioenergy Supply Systems" (Award Number EE0007088).

Appendix A. Supplementary material

Supplementary data to this article can be found online at https://doi.org/10.1016/j.compag.2019.105088.

References

American Society of Agricultural and Biological Engineers, 2015. Agricultural Machinery Management. ASABE, St. Joseph, MI, p. 1.

Bilal, M., Asgher, M., Iqbal, H.M., Hu, H., Zhang, X., 2017. Biotransformation of lignocellulosic materials into value-added products—a review. Int. J. Biol. Macromol. 98, 447–458.

Bonner, I., McNunn, G., Muth, D., Tyner, W., Leirer, J., Dakins, M., 2016. Development of integrated bioenergy production systems using precision conservation and multi-criteria decision analysis techniques. J. Soil Water Conserv. 71, 182–193.

Brandes, E., McNunn, G.S., Schulte, L.A., Muth, D.J., VanLoocke, A., Heaton, E.A., 2018. Targeted subfield switchgrass integration could improve the farm economy, water quality, and bioenergy feedstock production. GCB Bioenergy 10, 199–212.

Cai, H., Benavides, T., Lee, U., Wang, M., Tan, E., Davis, R., Dutta, A., Biddy, M., Clippinger, J., Grundl, N., 2018. Supply Chain Sustainability Analysis of Renewable Hydrocarbon Fuels via Indirect Liquefaction, Ex Situ Catalytic Fast Pyrolysis, Hydrothermal Liquefaction, Combined Algal Processing, and Biochemical Conversion: Update of the 2018 State-of-Technology Cases and Design Cases. Argonne National Lab.(ANL), Argonne, IL (United States).

Cibin, R., Trybula, E., Chaubey, I., Brouder, S.M., Volenec, J.J., 2016. Watershed-scale impacts of bioenergy crops on hydrology and water quality using improved SWAT model. GCB Bioenergy 8, 837–848.

Douglas, J., Lemunyon, J., Wynia, R., Salon, P., 2009. Planting and managing switchgrass as a biomass energy crop. Natural Resources Conservation Service, US Department of Agriculture, Technical Note.

Estrada-Carmona, N., Hart, A.K., DeClerck, F.A., Harvey, C.A., Milder, J.C., 2014. Integrated landscape management for agriculture, rural livelihoods, and ecosystem conservation: an assessment of experience from Latin America and the Caribbean. Landscape Urban Plann. 129, 1–11.

Gelfand, I., Sahajpal, R., Zhang, X.S., Izaurralde, R.C., Gross, K.L., Robertson, G.P., 2013. Sustainable bioenergy production from marginal lands in the US Midwest. Nature 493, 514-+.

Gonzalez, X.P., Alvarez, C.J., Crecente, R., 2004. Evaluation of land distributions with joint regard to plot size and shape. Agric. Syst. 82, 31–43.

Ha, M., Wu, M., 2015. Simulating and evaluating best management practices for integrated landscape management scenarios in biofuel feedstock production. Biofuels Bioprod. Biorefin. 9, 709–721.

Isikgor, F.H., Becer, C.R., 2015. Lignocellulosic biomass: a sustainable platform for the production of bio-based chemicals and polymers. Polym. Chem. 6, 4497–4559.

Langholtz, M.H., Stokes, B.J., Eaton, L.M., Brandt, C.C., Davis, M.R., Theiss, T.J., Turhollow Jr, A.F., Webb, E., Coleman, A., Wigmosta, M., 2016. 2016 Billion-ton report: advancing domestic resources for a thriving bioeconomy, volume 1: economic availability of feedstocks. Oak Ridge National Lab.(ORNL), Oak Ridge, TN (United States).

Liebig, M.A., Johnson, H.A., Hanson, J.D., Frank, A.B., 2005. Soil carbon under switchgrass stands and cultivated cropland. Biomass Bioenergy 28, 347–354.

Luck, J., Zandonadi, R., Shearer, S., 2011. A case study to evaluate field shape factors for estimating overlap errors with manual and automatic section control. Trans. ASABE 54, 1237–1243.

McLaughlin, S.B., Kszos, L.A., 2005. Development of switchgrass (Panicum virgatum) as a bioenergy feedstock in the United States. Biomass Bioenergy 28, 515–535.

Nair, S.K., Griffel, L.M., Hartley, D.S., McNunn, G.S., Kunz, M.R., 2018. Investigating the efficacy of integrating energy crops into non-profitable subfields in Iowa. Bioenergy Res. 11, 623–637.

Oksanen, T., 2013. Shape-describing indices for agricultural field plots and their relationship to operational efficiency. Comput. Electron. Agric. 98, 252–259.

Parrish, D.J., Fike, J.H., 2005. The biology and agronomy of switchgrass for biofuels. Crit. Rev. Plant. Sci. 24, 423–459.

Pedregosa, F., Varoquaux, G., Gramfort, A., Michel, V., Thirion, B., Grisel, O., Blondel, M., Prettenhofer, P., Weiss, R., Dubourg, V., 2011. Scikit-learn: machine learning in Python. J. Mach. Learn. Res. 12, 2825–2830.

QGIS Development Team, 2018. QGIS Geographic Information System. Open Source. Geospatial Foundation Project.

Robertson, B.A., Doran, P.J., Loomis, L.R., Robertson, J.R., Schemske, D.W., 2011. Perennial biomass feedstocks enhance avian diversity. GCB Bioenergy 3, 235–246.

Roni, M., Hansen, J., Griffel, M., Hartley, D., Mamun, S., Vazhnik, V., 2018. Enabling Sustainable Landscape Design for Continual Improvement of Operating Bioenergy Supply Systems (INL/MIS-18-51176). Idaho National Laboratory, Idaho Falls, Idaho, USA.

Sayer, J., Sunderland, T., Ghazoul, J., Pfund, J.-L., Sheil, D., Meijaard, E., Venter, M., Boedhihartono, A.K., Day, M., Garcia, C., 2013. Ten principles for a landscape approach to reconciling agriculture, conservation, and other competing land uses. Proc. Natl. Acad. Sci. 110, 8349–8356.

Schulte, L.A., Niemi, J., Helmers, M.J., Liebman, M., Arbuckle, J.G., James, D.E., Kolka, R.K., O'Neal, M.E., Tomer, M.D., Tyndall, J.C., Asbjornsen, H., Drobney, P., Neal, J., Van Ryswyk, G., Witte, C., 2017. Prairie strips improve biodiversity and the delivery of multiple ecosystem services from corn-soybean croplands. Proc. Natl. Acad. Sci. USA 114, 11247–11252.

Seabold, S., Perktold, J., 2010. Statsmodels: econometric and statistical modeling with python. In: Proceedings of the 9th Python in Science Conference. Scipy, pp. 61.

Sokhansanj, S., Mani, S., Turhollow, A., Kumar, A., Bransby, D., Lynd, L., Laser, M., 2009. Large-scale production, harvest and logistics of switchgrass (Panicum virgatum L.) - current technology and envisioning a mature technology. Biofuel Bioprod. Bior. 3, 124–141.

Ssegane, H., Negri, M.C., 2016. An integrated landscape designed for commodity and bioenergy crops for a tile-drained agricultural watershed. J. Environ. Qual. 45, 1588–1596.

Toussaint, G.T., 1983. Solving geometric problems with the rotating calipers. In: Proc. IEEE Melecon, pp. A10.

United States Department of Transporation, 2008. Global Positioning System Wide Area Augmentation System (WAAS) Performance Standard, first ed.

Velandia, M., Buschermohle, M., Larson, J.A., Thompson, N.M., Jernigan, B.M., 2013. The economics of automatic section control technology for planters: A case study of middle and west Tennessee farms. Comput. Electron. Agric. 95, 1–10.

Werling, B.P., Dickson, T.L., Isaacs, R., Gaines, H., Gratton, C., Gross, K.L., Liere, H., Malmstrom, C.M., Meehan, T.D., Ruan, L.L., Robertson, B.A., Robertson, G.P., Schmidt, T.M., Schrotenboer, A.C., Teal, T.K., Wilson, J.K., Landis, D.A., 2014. Perennial grasslands enhance biodiversity and multiple ecosystem services in bioenergy landscapes. P. Natl. Acad. Sci. USA 111, 1652–1657.

Wold, M.T., Kocher, M.F., Keshwani, D.R., Jones, D.D., 2011. Modeling the In-Field Logistics of Single Pass Crop Harvest and Residue Collection, 2011 Louisville, Kentucky, August 7–10, 2011. ASABE, St. Joseph, MI.

Zhou, K., Jensen, A.L., Sorensen, C.G., Busato, P., Bothtis, D.D., 2014. Agricultural operations planning in fields with multiple obstacle areas. Comput. Electron. Agric. 109, 12–22.